

BF-STVSR: B-Splines and Fourier—Best Friends for High Fidelity Spatial-Temporal Video Super-Resolution

Eunjin Kim^{*1}, Hyeonjin Kim^{*1}, Kyong Hwan Jin², and Jaejun Yoo¹

¹Ulsan National Institute of Science and Technology (UNIST)

²Korea University

Abstract

Enhancing low-resolution, low-frame-rate videos to high-resolution, high-frame-rate quality is essential for a seamless user experience, motivating advancements in Continuous Spatial-Temporal Video Super Resolution (C-STVSR). While prior methods employ Implicit Neural Representation (INR) for continuous encoding, they often struggle to capture the complexity of video data, relying on simple coordinate concatenation and pre-trained optical flow network for motion representation. Interestingly, we find that adding position encoding, contrary to common observations, does not improve—and even degrade—performance. This issue becomes particularly pronounced when combined with pre-trained optical flow networks, which can limit the model’s flexibility. To address these issues, we propose **BF-STVSR**, a C-STVSR framework with two key modules tailored to better represent spatial and temporal characteristics of video: 1) B-spline Mapper for smooth temporal interpolation, and 2) Fourier Mapper for capturing dominant spatial frequencies. Our approach achieves state-of-the-art PSNR and SSIM performance, showing enhanced spatial details and natural temporal consistency. Our code will be available soon.

1. Introduction

Enhancing low-resolution, low-frame-rate videos to high-resolution, high-frame-rate quality is crucial for delivering seamless user experiences. To address this, deep learning approaches for Video Super-Resolution (VSR) [3, 4, 43, 44, 46] and Video Frame Interpolation (VFI) [1, 8–10, 13, 18, 38, 47, 50] have been extensively studied. VSR typically enhances spatial resolution of target frames by leveraging information from neighboring frames, while VFI improves temporal resolution by predicting inherent motion

^{*}Equal contribution

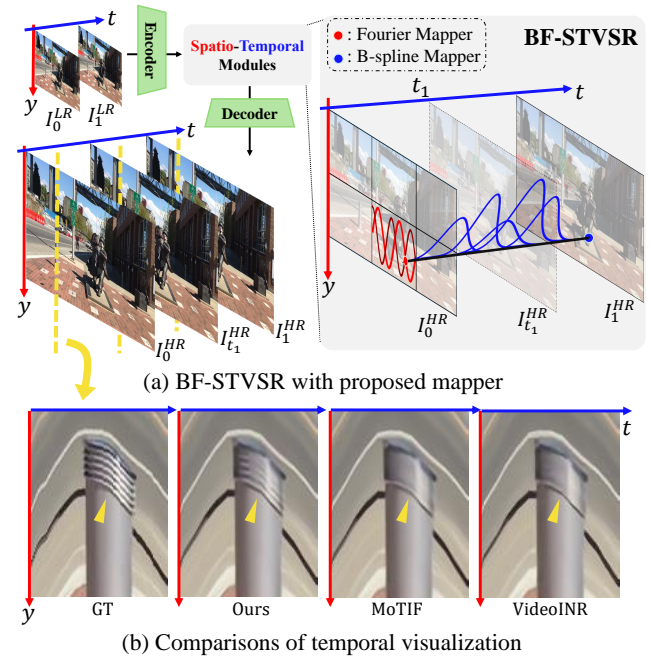


Figure 1. Illustration of BF-STVSR and results. (a) BF-STVSR captures the high-frequency spatial feature by Fourier Mapper and interpolates temporal information smoothly via B-spline Mapper. (b) Temporal visualization of the interpolated video. We visualize the changes of the interpolated frames over time t for a selected x -axis (indicated by yellow vertical line in (a)).

in video data. However, many existing methods are limited by fixed scaling factors set during training, which restricts their flexibility in real-world applications.

On the other hand, Implicit Neural Representation (INR) has recently garnered attention for its capability to represent signals continuously through a multi-layer perceptron (MLP), making it a promising approach for super-resolution (SR) tasks [5, 15, 22, 32]. Building on these advancements,

recent studies have extended INR to video data to achieve Continuous Spatial-Temporal Video Super Resolution (C-STVSR), which enables spatial and temporal interpolation simultaneously at arbitrary scales [6, 7]. VideoINR [7] was the first method to map spatiotemporal coordinates (x, y, t) to backward motion field, facilitating backward warping of spatial features to any temporal coordinate. MoTIF [6] improved on this by replacing the backward warping with forward warping, using softmax splatting [31]. In addition, to facilitate the learning in an explicit way, MoTIF supply forward optical flow maps estimated between reference frames as contextual information, using RAFT [42].

While VideoINR and MoTIF successfully integrate INR into the C-STVSR task, they have notable limitations. Specifically, they generate target features by encoding latent features that are simply concatenated with target coordinates, without employing advanced position encoding techniques. This is surprising, given that various position encoding methods—such as Fourier encoding [27, 41]—are well-established and widely used in tasks like image SR with INR due to their effectiveness, having become a conventional process [16, 22, 32, 48]. This straightforward approach may fall short in capturing the nuanced details of spatial and temporal features, especially for motion features, which are inherently complex and dynamic. Consequently, both models struggle to retain high-frequency information in the encoded spatial features, a well-known limitation referred to as spectral bias [34, 41], resulting in the generation of lower-quality frames.

Interestingly, however, we find that simply adding position encoding does not improve—and even degrade—performance in these models, an unexpected outcome that contrasts with the general success of position encoding in enhancing INR applications [12, 19, 28, 45]. This issue becomes particularly pronounced when combined with pre-trained optical flow networks. We conjecture that, while these networks provide useful guidance for motion representation, integrating them with position encoding can inadvertently limit the model’s flexibility to fully leverage diverse video information.

To address these limitations, we propose BF-STVSR, a framework consisting of two modules: B-spline Mapper (BM) and Fourier Mapper (FM), each designed to handle temporal and spatial features. First, B-spline Mapper (BM) utilizes B-spline function, well-known established method for constructing smooth curves or surfaces [32]. This approach well-suited for capturing the continuous nature of video motion. Next, Fourier Mapper (FM) represents spatial features by estimating dominant frequency information of input video frames, effectively capturing fine details. Additionally, based on our earlier analysis, rather than directly integrating a pre-trained optical flow network into our framework, we incorporate it implicitly as a loss function

during training to guide the network. This design allows the model to fully leverage the rich information inherent in video data, yielding enhanced interpolated outputs.

In summary, our contributions are as follows: (1) We propose BF-STVSR, a framework that independently address the spatial and temporal axes by leveraging their distinct characteristics. To achieve this, (2) we design two dedicated components, B-spline Mapper (BM) for temporal motion representation and Fourier Mapper (FM) for spatial feature representation. (3) We achieve state-of-the-art performance in C-STVSR, demonstrating the effectiveness of our approach through extensive experiments.

2. Related Work

2.1. Arbitrary Single Image Super Resolution

Single Image Super Resolution (SISR) methods [23, 24, 37, 54] have achieved impressive performance, but their reliance on fixed scales limits their applicability in real-world scenarios. To address this, several studies have proposed methods to perform super resolution at arbitrary scales [5, 22, 26, 32, 51]. LIIF [5] introduced an Implicit Neural Representation (INR) approach for super resolution, representing images continuously through local implicit functions and enabling arbitrary scale upsampling. [26, 51] further used position encoding to address the spectral bias problem [34]. Recently, LTE [22] proposed identifying dominant Fourier bases from latent features to effectively capture fine details and address spectral bias. Similarly, BTC [32] employed B-spline bases instead of Fourier bases to mitigate the Gibbs phenomenon observed in Screen Content Image Super Resolution. Inspired by these methods, we explore effective position encoding techniques for C-STVSR task, which reflect the characteristics of video data.

2.2. Spatial-Temporal Video Super Resolution

While conventional Video Super-Resolution (VSR) [2–4, 36] and Video Frame Interpolation (VFI) [8–11, 13, 18, 20, 21, 30, 31, 33, 35, 38, 53] perform interpolation along either spatial or temporal axis, Spatial-Temporal Video Super Resolution (STVSR) conducts interpolation along both axes. Haris *et al.* [14] have introduced a unified framework for addressing STVSR and Xiang *et al.* [47] have proposed to use bidirectional deformable ConvLSTM. Although these studies demonstrate impressive performance in STVSR, they both have the limitation of only addressing STVSR at fixed scales. Recently, two works [6, 7] have been proposed for Continuous Spatial-Temporal Video Super Resolution (C-STVSR), which performs interpolation at arbitrary scales along both spatial and temporal axes. VideoINR [7] is the first work on C-STVSR, which takes space-time coordinates as input and maps the corresponding RGB value in continuous manner using INR. Following

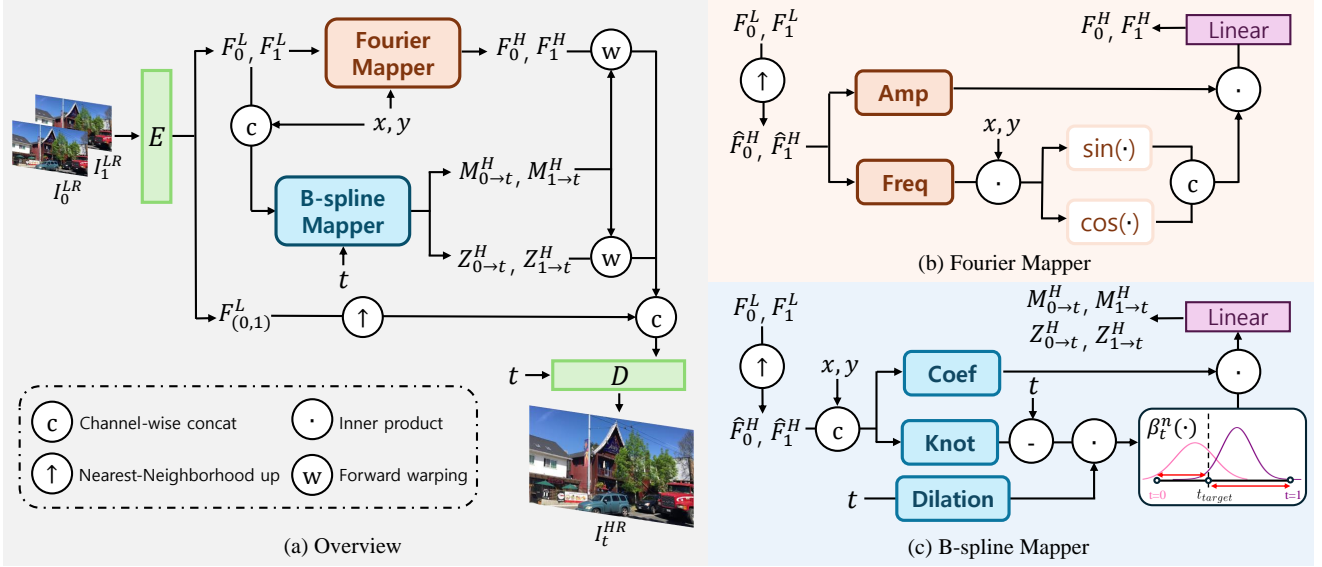


Figure 2. **Schematic overview of our BF-STVSR.** (a) First, two input frames are encoded as low-resolution feature maps. Based on these features, Fourier Mapper predicts the dominant frequency information, while B-spline Mapper predicts smoothly interpolated motion, which is then processed into optical flows at an arbitrary time t . The frequency information is temporally propagated by being warped with the optical flows. Finally, the warped frequency information is decoded to generate high-resolution interpolated RGB frame. (b) Fourier Mapper estimates the dominant frequency and its amplitude to capture fine-detail information from the given frames. (c) B-spline Mapper estimates B-spline coefficients to model inherent motion, which smoothly interpolates motion features temporally.

this, MoTIF [6] generates temporal features using optical flow and performs forward warping to predict the interpolated high-resolution frame features. Although these studies effectively tackle the C-STVSR task, relying solely on MLPs for spatial and temporal modeling leads to difficulties in learning the characteristics of the video. In this work, we adopt Fourier basis and B-spline basis functions to model spatial and temporal features of video data to address the aforementioned difficulties.

3. Method

3.1. Overview

The overall flow of our method, BF-STVSR, is illustrated in Figure 2 (a). Our framework is built upon the pipeline of MoTIF [6]. Given two low-resolution frames $I_0^L, I_1^L \in \mathbb{R}^{3 \times H \times W}$, our goal is to generate a high-resolution intermediate frame $I_t^H \in \mathbb{R}^{3 \times sH \times sW}$ at any time $t \in [0, 1]$ with an arbitrary scale s . The encoder E first takes the low-resolution frames as input and produces three latent features: $F_0^L, F_{(0,1)}^L, F_1^L \in \mathbb{R}^{C \times H \times W}$. Here, F_0^L and F_1^L represent the latent features of I_0^L and I_1^L , while $F_{(0,1)}^L$ serves as a template feature for the intermediate frame, incorporating information from both input frames. Next, the latent features F_0^L, F_1^L are processed by two mappers. The B-spline Mapper (Section 3.2) predicts high-resolution optical flows to target time t , producing $M_{0 \rightarrow t}^H, M_{1 \rightarrow t}^H \in$

$\mathbb{R}^{2 \times sH \times sW}$, while the Fourier Mapper (Section 3.3) estimates high-resolution spatial features at target scale s , resulting in $F_0^H, F_1^H \in \mathbb{R}^{C \times sH \times sW}$. Finally, the high-resolution features F_0^H, F_1^H are temporally propagated to the target time t using forward warping based on the predicted optical flow $M_{0 \rightarrow t}^H, M_{1 \rightarrow t}^H$, generating intermediate features F_t^H . These warped features are then concatenated with target time t and $F_{(0,1)}^H$, a nearest-neighbor upsampled version of $F_{(0,1)}^L$, and decoded to produce the high-resolution intermediate frame I_t^H .

3.2. Temporal B-spline Mapper

Accurately predicting the motion inherent in a video is key to generating a visually plausible intermediate frame from two neighboring frames. While various techniques have been proposed in video frame interpolation (VFI) studies [8, 11, 18, 20, 31, 33, 35, 53] to predict motion accurately, most of them are designed for fixed scale interpolation. Therefore, applying these methods to the C-STVSR task, which requires handling arbitrary scales, is not straightforward. To overcome this challenge, VideoINR [7] and MoTIF [6] use implicit neural representations (INR) with MLPs that take spatiotemporal coordinates as input, enabling motion modeling at arbitrary target times t and scales s . While INR-based motion modeling provides flexibility in motion prediction, we find that it often struggles to capture the complex, dynamic nature of motion in video.

To better represent inherent motion, we introduce B-spline Mapper, which leverages the B-spline representation. B-spline bases are widely known for their effectiveness in modeling continuous signals [32], making them well-suited for capturing smooth, continuous motion in videos, where objects move smoothly and continuously, rather than in jerky manner. The detailed process of B-spline Mapper is described in Figure 2 (b). We modify the Space-Time Local Implicit Neural Functions (ST-INF) from MoTIF [6], resulting in our B-spline Mapper. Similar to ST-INF, B-spline Mapper predicts high-resolution forward motion vectors $M_{0 \rightarrow t}^H, M_{1 \rightarrow t}^H$ and reliability maps $Z_{0 \rightarrow t}^H, Z_{1 \rightarrow t}^H$ at arbitrary time $t \in [0, 1]$. A key difference is that our B-spline Mapper takes encoded features F_0^L, F_1^L as input, rather than optical flows from an external network (e.g., RAFT [42]).

In addition, rather than directly predicting motion vectors to the target time t , our B-spline Mapper p_ψ models the video’s inherent motion by predicting the B-spline coefficients and knots, as described in the following equation:

$$p_\psi(z_r, \delta_r, \hat{t}) = c_r \odot \beta^n \left(\frac{\hat{t} - k_r}{d} \right). \quad (1)$$

Here, $c_r = p_c(z_r, \delta_r)$, $k_r = p_k(z_r, \delta_r)$, and $d = p_d(g)$. Specifically, $z_r = F_{t_r}^L(q_r)$ is the latent feature vector at the point $q_r = (x_r, y_r)$, nearest to the query coordinates $q = (x, y)$, with the reference frame time index $t_r \in \{0, 1\}$. The functions p_c, p_k , and p_d are the estimators for the coefficients ($\mathbb{R}^{C+2} \mapsto \mathbb{R}^C$), knots ($\mathbb{R}^{C+2} \mapsto \mathbb{R}^C$), and dilation ($\mathbb{R}^1 \mapsto \mathbb{R}^C$), respectively. $\hat{t} = |t - t_r|$ represents the relative temporal distance of the predicted feature to the reference frame, and $\delta_r (= q - q_r)$ is the spatial relative coordinate between the query and reference coordinates. Finally, g is the frame interval of the input video.

After linearly projecting the predicted B-spline representation using f_{θ_b} , we obtain the motion vector $Z_{t_r \rightarrow t}^H(q)$ and reliability map $M_{t_r \rightarrow t}^H(q)$ at the query coordinates q :

$$\{Z_{t_r \rightarrow t}^H(q), M_{t_r \rightarrow t}^H(q)\} = f_{\theta_b}(p_\psi(z_r, \delta_r, \hat{t})). \quad (2)$$

Using the predicted motion vectors, the spatial features F_0^H, F_1^H and reliability maps are propagated to the target time t via forward warping using softmax splatting [31]. Finally, we obtain intermediate latent feature F_t^H and corresponding reliability map Z_t^H . By directly learning the underlying motion from the input frames instead of individually predicting each arbitrary time t , our B-spline Mapper provides a more robust and flexible motion modeling approach. Additionally, since our method does not rely on optical flow inference during the inference stage, it is more efficient compared to previous approaches like MoTIF [6].

3.3. Spatial Fourier Mapper

Even with the robust motion modeling provided by the B-spline Mapper, the quality of the interpolated feature F_t^H

depends significantly on the features propagated from F_0^H and F_1^H . VideoINR [7] and MoTIF [6] rely on simple MLPs to interpolate the latent features F_0^L and F_1^L . However, implicit neural functions often struggle with capturing high-frequency details, leading to poor quality in the interpolated features, as noted in several studies [27, 34, 41]. To address this issue, LTE [22] demonstrated that using Fourier bases for spatial feature modeling significantly improves performance in arbitrary-scale super-resolution by effectively capturing dominant frequencies. Inspired by this approach, we integrate a similar strategy into our Fourier Mapper. The detail process is illustrated in Figure 2 (c). The Fourier Mapper g_ϕ predicts the dominant frequency and its amplitude of the Fourier bases for spatial features:

$$\{F_0^H(q), F_1^H(q)\} = f_{\theta_f}(g_\phi(z_r, \delta_r)), \quad (3)$$

$$\text{where } g_\phi(z_r, \delta_r) = A_r \odot \begin{bmatrix} \cos(\pi F_r \delta_r) \\ \sin(\pi F_r \delta_r) \end{bmatrix}. \quad (4)$$

Here, $A_r = g_a(z_r)$ and $F_r = g_f(z_r)$. Same as B-spline Mapper, $z_r = F_{t_r}^L(q_r)$ is the nearest latent feature vector from the query coordinates $q = (x, y)$ and $\delta_r (= q - q_r)$ is the relative coordinates in spatial domain. The g_a and g_f are the amplitude estimator ($\mathbb{R}^C \mapsto \mathbb{R}^{2C}$) and the frequency estimator ($\mathbb{R}^C \mapsto \mathbb{R}^{2C}$), respectively. By predicting dominant frequencies of query points in latent space, Fourier Mapper improves the frequency details of the interpolated features \hat{F}_0^H and \hat{F}_1^H . After all, by linearly projecting it to F_0^H and F_1^H using f_{θ_f} , which in turn enhances the quality of F_t^H . Note that, unlike LTE, which interpolates the estimated amplitude and frequency from low-resolution domain, our method estimates each coefficients in high-resolution domain and does not estimate the phase.

3.4. Training Objective

We follow [6] to train our model end-to-end :

$$\mathcal{L} = \mathcal{L}_{\text{char}}(\hat{I}_t^H, I_t^H) + \beta \sum_{i=0}^1 \mathcal{L}_{\text{char}}(\hat{M}_{i \rightarrow t}^H, M_{i \rightarrow t}^H), \quad (5)$$

where $\mathcal{L}_{\text{char}}$ is Charbonnier loss and β is a hyper-parameter which set as 0.01. The \hat{I}_t^H is the ground-truth high-resolution frame at time t and $\hat{M}_{i \rightarrow t}^H$ is the predicted optical flow from the RAFT [42]. Note that we use RAFT only to guide our B-spline Mapper during training.

4. Experiments

4.1. Experiments Setup

Implementation and Training Details To our knowledge, VideoINR [7] and MoTIF [6] are the only models addressing C-STVSR. Since both models employ identical training and testing scheme, we follow the same approach

Table 1. Performance comparison on the Fixed-scale STVSR baselines on Vid4, Gopro, and Adobe240 datasets. Results are evaluated using PSNR (dB) and SSIM metrics. All frames are interpolated by a factor of $\times 4$ in the spatial axis and $\times 8$ in the temporal axis. “Average” refers to metrics calculated across all 8 interpolated frames, while “Center” refers to metrics measured using 1^{st} , 4^{th} and 9^{th} (that is single-frame interpolation) frames of the interpolated sequence. **Red** and **blue** indicate the best and the second best performance, respectively.

VFI Method	VSR Method	Vid4	Gorpo-Center	Gopro-Average	Adobe-Center	Adobe-Average	Parameters (Millions)
SuperSloMo [17]	Bicubic	22.42 / 0.5645	27.04 / 0.7937	26.06 / 0.7720	26.09 / 0.7435	25.29 / 0.7279	19.8
SuperSloMo [17]	EDVR [46]	23.01 / 0.6136	28.24 / 0.8322	26.30 / 0.7960	27.25 / 0.7972	25.90 / 0.7682	19.8+20.7
SuperSloMo [17]	BasicVSR [3]	23.17 / 0.6159	28.23 / 0.8308	26.36 / 0.7977	27.28 / 0.7961	25.94 / 0.7679	19.8+6.3
QVI [50]	Bicubic	22.11 / 0.5498	26.50 / 0.7791	25.41 / 0.7554	25.57 / 0.7324	24.72 / 0.7114	29.2
QVI [50]	EDVR [46]	23.48 / 0.6547	28.60 / 0.8417	26.64 / 0.7977	27.45 / 0.8087	25.64 / 0.7590	29.2+20.7
QVI [50]	BasicVSR [3]	23.15 / 0.6428	28.55 / 0.8400	26.27 / 0.7955	26.43 / 0.7682	25.20 / 0.7421	29.2+6.3
DAIN [1]	Bicubic	22.57 / 0.5732	26.92 / 0.7911	26.11 / 0.7740	26.01 / 0.7461	25.40 / 0.7321	24.0
DAIN [1]	EDVR [46]	23.48 / 0.6547	28.58 / 0.8417	26.64 / 0.7977	27.45 / 0.8087	25.64 / 0.7590	24.0+20.7
DAIN [1]	BasicVSR [3]	23.43 / 0.6514	28.46 / 0.7966	26.43 / 0.7966	26.23 / 0.7725	25.23 / 0.7725	24.0+6.3
ZoomingSloMo [47]		25.72 / 0.7717	30.69 / 0.8847	- / -	30.26 / 0.8821	- / -	11.10
TMNet [49]		25.96 / 0.7803	30.14 / 0.8696	28.83 / 0.8514	29.41 / 0.8524	28.30 / 0.8354	12.26
VideoINR [7]		25.61 / 0.7709	30.26 / 0.8792	29.41 / 0.8669	29.92 / 0.8746	29.27 / 0.8651	11.31
MoTIF [6]		25.79 / 0.7745	31.04 / 0.8877	30.04 / 0.8773	30.63 / 0.8839	29.82 / 0.8750	12.55
Ours		25.80 / 0.7754	31.14 / 0.8893	30.20 / 0.8799	30.84 / 0.8877	30.14 / 0.8808	12.68

Table 2. Performance comparison on the C-STVSR baselines for out-of-distribution scale on Gopro dataset. Results are evaluated using PSNR (dB) and SSIM metrics. All frames are interpolated by a scaling factor specified on the table and metrics calculated across all interpolated frames. **Bold** indicates the best performance.

Temporal Scale	Spatial Scale	SuperSloMo [17] + LIIF [5]	DAIN [1] + LIIF [5]	TMNet [49]	VideoINR [7]	MoTIF [6]	Ours
$\times 8$	$\times 4$	-	-	28.83 / 0.8514	29.41 / 0.8669	30.04 / 0.8773	30.20 / 0.8799
$\times 6$	$\times 4$	26.70 / 0.7988	26.71 / 0.7998	30.49 / 0.8861	30.78 / 0.8954	31.56 / 0.9064	31.68 / 0.9082
$\times 6$	$\times 6$	23.47 / 0.6931	23.36 / 0.6902	-	25.56 / 0.7671	29.36 / 0.8505	29.44 / 0.8516
$\times 6$	$\times 12$	21.92 / 0.6495	22.01 / 0.6499	-	24.02 / 0.6900	25.81 / 0.7330	25.78 / 0.7284
$\times 12$	$\times 4$	25.07 / 0.7491	25.14 / 0.7497	26.38 / 0.7931	27.32 / 0.8141	27.77 / 0.8230	28.06 / 0.8287
$\times 12$	$\times 6$	22.91 / 0.6783	22.92 / 0.6785	-	24.68 / 0.7358	26.78 / 0.7908	27.06 / 0.7961
$\times 12$	$\times 12$	21.61 / 0.6457	21.78 / 0.6473	-	23.70 / 0.6830	24.72 / 0.7108	24.87 / 0.7096
$\times 16$	$\times 4$	24.42 / 0.7296	24.20 / 0.7244	24.72 / 0.7526	25.81 / 0.7739	25.98 / 0.7758	26.40 / 0.7844
$\times 16$	$\times 6$	23.28 / 0.6883	22.80 / 0.6722	-	23.86 / 0.7123	25.34 / 0.7527	25.81 / 0.7621
$\times 16$	$\times 12$	21.80 / 0.6481	22.22 / 0.6420	-	22.88 / 0.6659	23.88 / 0.6923	24.22 / 0.6950

unless otherwise noted. We adopt the same two-stage training strategy: for the first 450,000 iterations, the spatial scaling factor is fixed as 4, while for the remaining 150,000 iterations, it is uniformly sampled from [1, 4]. We use the Adam optimizer with parameters $\beta_1 = 0.9$ and $\beta_2 = 0.999$, and apply cosine annealing to decay the learning rate from 10^{-4} to 10^{-7} for every 150,000 iterations. ZoomingSlowMo [47] is used as the encoder, with a batch size of 32, and random rotation and horizontal-flipping for data augmentation. To ensure training stability, we substitute the predicted forward motion with the ground-truth forward motion with a certain probability, starting from 1.0 and gradually reducing to 0 over the first 150,000 iterations. For B-spline Mapper, we use the three-layer SIRENs as the coefficient and knot estimators, and a single fully connected layer as the dilation estimator. In Fourier Mapper, we use three-layer SIRENs as the amplitude and frequency estimators, followed by a 3×3 convolution for spatial encoding. Both B-spline Map-

per and Fourier Mapper have hidden dimensions of 64, with SIREN layer dimensions set to 64, 64, and 256.

Datasets We use the Adobe240 dataset [40] for training, which consists of 133 videos in 720P taken by hand-held cameras. We split these videos into 100 for training, 16 for validation, and 17 for test. During training, nine sequential frames are selected from the video and the 1^{st} and 9^{th} frames are used as input reference frames. Three frames are then randomly sampled between them and used as the target ground-truth frames. For evaluation, we use Vid4[25], Adobe240 [39], and Gopro [29] datasets. Unless otherwise specified, the default spatial scale is 4, while the temporal scaling factor varies across datasets. For Vid4, temporal scale is set to $\times 2$ corresponding to single frame interpolation. For Adobe240-Average and Gopro-Average, the temporal scale is set as $\times 8$, representing multi-frame interpolation. Additionally, for Adobe240-center and Gopro-Center,

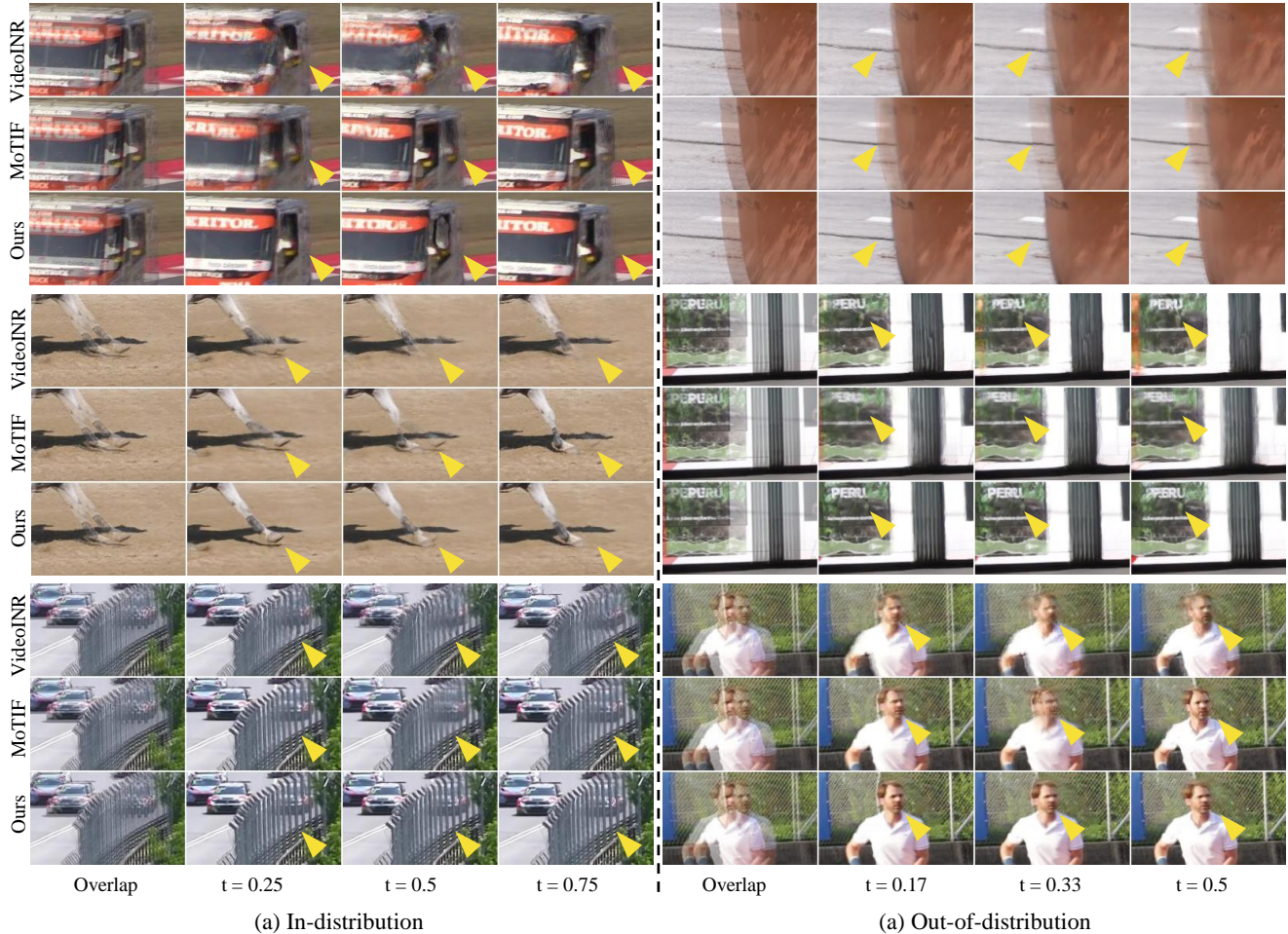


Figure 3. Qualitative comparison on arbitrary scale temporal interpolation. “Overlap” refers to the averaged image of two input frames ($t = 0, 1$), and the following images are interpolation results at $t = (0, 1)$. (a) shows the interpolated results on in-distribution time scale ($\times 8$), used during training. (b) shows the out-of-distribution time scale ($\times 6$), not seen during training.

Table 3. Comparison of the degradation gap as the scale increases with various arbitrary scales in both axes. We measure the performance drop when the temporal scale is increased compared to the temporal scale $\times 6$ at the corresponding spatial scale. Results are evaluated using PSNR (dB) and SSIM metrics. The larger (-) value means greater performance degradation.

Spatial scale	$\times 4$			$\times 6$			$\times 12$		
Temporal scale	$\times 6$	$\Delta(\times 12)$	$\Delta(\times 16)$	$\times 6$	$\Delta(\times 12)$	$\Delta(\times 16)$	$\times 6$	$\Delta(\times 12)$	$\Delta(\times 16)$
MoTIF [6]	31.56 / 0.906	-3.79 / -0.083	-5.58 / -0.130	29.36 / 0.850	-2.58 / -0.059	-4.02 / -0.097	25.81 / 0.733	-1.09 / -0.022	-1.93 / -0.040
Ours	31.68 / 0.908	-3.62 / -0.079	-5.28 / -0.123	29.44 / 0.851	-2.38 / -0.055	-3.63 / -0.089	25.78 / 0.728	-0.91 / -0.018	-1.56 / -0.033

evaluation is performed only on the center frames (*i.e.*, the 1st, 4th, 9th frames).

Baseline methods We categorize baseline models into two types—continuous and fixed-scale—and conduct comparisons within each category. Here, Fixed-scale Space-Time Video Super-Resolution (Fixed-STVSR) are limited to super-resolving at fixed scaling factors in both axes that are learned during the training. First, we select two-stage Fixed-STVSR methods that combine fixed video super-

resolution models (*e.g.*, Bicubic Interpolation, EDVR [46], BasicVSR [3]) with video frame interpolation models (*e.g.*, SuperSloMo [17], QVI [50], DAIN [1]). Second, we select one-stage Fixed-STVSR method, specifically ZoomingSlowMo [47]. For continuous methods, we select two-stage C-STVSR methods that combine continuous image super-resolution models (*e.g.*, LIIF [5]) with video frame interpolation models (*e.g.*, SuperSloMo [17], DAIN [1]). Lastly, we select one-stage C-STVSR methods, including TMNet [49], VideoINR [7], and MoTIF[6]. Note that TM-

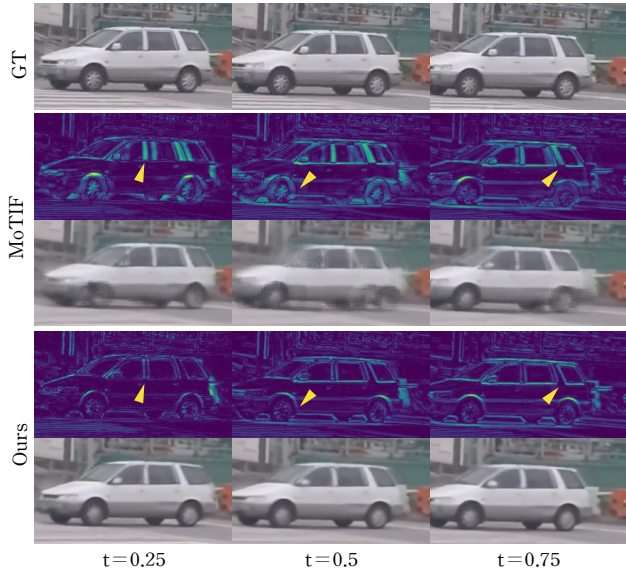


Figure 4. Qualitative comparison on a large out-of-distribution scale with a spatial scale of $\times 4$ and a temporal scale of $\times 12$. Three interpolation results at $t = 0.25, 0.5, 0.75$ are shown with residual intensity maps compared to the ground truth frame.

Net is limited to $\times 4$ spatial super-resolution.

Metrics We use Peak Signal-to-Noise Ratio (PSNR) and Structural Similarity Index (SSIM) on the Y channel to evaluate the model performance.

4.2. Quantitative results

We compare our model with Fixed-STVSR methods in Table 1. For single-frame interpolation tasks in STVSR, including Vid4, GoPro-*Center*, and Adobe-*Center*, our model achieves the best performance on all datasets except Vid4. On Vid4, TMNet outperforms other models, likely due to its training on the Vimeo90K dataset [52], which has characteristics similar to Vid4. For multi-frame interpolation tasks in STVSR, represented by GoPro-*Average* and Adobe-*Average*, our model surpasses the performance of the state-of-the-art MoTIF model, which uses a pre-trained optical flow network [42] to generate temporal features during training. This improvement suggests that the B-spline Mapper and Fourier Mapper components in our model provide more robust temporal and spatial feature representations.

Additionally, we compare our model with C-STVSR methods in Table 2, focusing on arbitrary-scales that were not seen during training. We perform experiments on GoPro dataset. Note that while TMNet supports continuous frame interpolation, it is limited to $\times 4$ spatial super-resolution. Our results show that BF-STVSR achieves the best performance across all test cases, except for a minor disparity (0.03 dB lower PSNR) at $\times 6$ temporal scale and $\times 6$

Table 4. The impact of different position embeddings and the pre-trained optical flow network. We compare various configurations on GoPro and Adobe datasets, following the setting of *Average* in Table 1. **O-F** denotes the pre-trained optical flow network [42], **B** represents B-spline Mapper and **F** represents Fourier Mapper. Results are evaluated using PSNR (dB) and SSIM metrics.

O-F	B	F	GoPro	Adobe
✓			30.04 / 0.8773	29.82 / 0.8750
✓		✓	29.94 / 0.8764	29.73 / 0.8741
✓	✓		30.03 / 0.8774	29.81 / 0.8756
		✓	30.12 / 0.8783	30.02 / 0.8784
	✓		30.16 / 0.8792	30.11 / 0.8801
	✓	✓	30.20 / 0.8799	30.14 / 0.8808

spatial scale. This finding suggests that our B-spline Mapper effectively handles temporal interpolation even at distant time intervals. Based on Table 2, we present the performance degradation in PSNR and SSIM as the temporal scale increases from $\times 6$ to $\times 12$ and $\times 16$ across various spatial scales in Table 3. Our results demonstrate that MoTIF experiences a more pronounced performance drop than our model under challenging conditions. Specifically, at $\times 12$ spatial scale, as the temporal scale increases from $\times 6$ to $\times 12$, MoTIF shows a degradation of approximately -4.02 dB, while our model degrades by around -3.63 dB, indicating an improvement of nearly 0.4 dB. This suggests that our method remains robust even under extreme conditions, with temporal intervals extending up to $\times 16$.

4.3. Qualitative results

In Figure 3, qualitative results are shown, comparing our model with VideoINR and MoTIF. The results include interpolated frames for an in-distribution temporal scale ($\times 8$), used during training (left), and an out-of-distribution temporal scale ($\times 6$), unseen during training (right). For the in-distribution scale, BF-STVSR captures high-frequency details more effectively, particularly in the horse’s hooves and the striped shape of the handrails. For the out-of-distribution scale, BF-STVSR demonstrates superior performance in dynamic motion scenes, accurately interpolating edges of the text and the man’s face, where other methods produce blurry or ghosted frames. These results highlight our model’s ability to perform natural motion interpolation for moving objects while effectively preserving high-frequency details. Additionally, Figure 4 shows interpolated results at an extreme scale with a spatial scale of $\times 4$ and a temporal scale of $\times 12$. We include interpolated frames at sampled time points ($t = 0.25, 0.5, 0.75$) along with residual intensity maps compared to ground truth frames. Our method produces sharper and more accurate results than MoTIF, especially in areas like the tire and the region next to the car window. Additional results for all time coordi-

Table 5. Ablation study on the cross basis function configurations. Results are evaluated using PSNR (dB) and SSIM metrics. “Ours-cross” uses Fourier Mapper as temporal basis function and B-spline Mapper as spatial basis function. “Ours-FF” uses Fourier Mapper for both axes and “Ours-BB” uses B-spline Mapper for both axes. **Bold** indicates the best performance.

	Vid4	Gopro-Center	Gopro-Average	Adobe-Center	Adobe-Average
Ours	25.80 / 0.7754	31.14 / 0.8893	30.20 / 0.8799	30.84 / 0.8877	30.14 / 0.8808
Ours-cross	25.78 / 0.7747	31.10 / 0.8892	30.17 / 0.8796	30.80 / 0.8876	30.10 / 0.8804
Ours-FF	25.79 / 0.7750	31.12 / 0.8894	30.18 / 0.8798	30.84 / 0.8879	30.13 / 0.8809
Ours-BB	25.82 / 0.7753	31.07 / 0.8885	30.16 / 0.8793	30.77 / 0.8865	30.09 / 0.8797

ates are provided in the supplementary document.

4.4. Ablation Study

Optical Flow and Position Embeddings Table 4 compares model performance with and without pre-trained optical flow network, RAFT [42], across different combinations of our proposed B-spline Mapper and Fourier Mapper modules. The first row shows the basic MoTIF [6] configuration. As seen in the second and third row, including the optical flow network with the proposed modules degrades performance. In contrast, directly using the proposed modules to extract spatial and temporal features, without the optical flow network, improves performance across all cases (last three rows). We attribute this improvement to the proposed modules facilitating the model’s effective extraction and utilization of the rich information embedded within the video, enhancing its capacity to capture complex spatial and temporal features. In addition, the fourth and fifth row in Table 4 represent the impact of the B-spline Mapper and Fourier Mapper, respectively. The fourth row is the result of using only Fourier Mapper for spatial feature encoding at BF-STVSR (last row) simply mapping the counterpart axis by concatenating latent features with target coordinates. which termed as Ours-F. The fifth row is the result of using only B-spline Mapper for temporal feature encoding at BF-STVSR (last row), which termed as Ours-B. As shown in the table, performance decreases when each mapper is used independently, but the best results are achieved when both mappers are integrated.

Different basis functions We conduct additional experiments by varying the basis functions used for both axes (Table 5). In all configurations, the basis function model the spatial and temporal axes, while other components (*e.g.*, linear projection for intermediate motion vectors and reliability maps) remain the same. Although the performance differences among these configurations are minimal (around 0.04 dB), we adopt the configuration using B-spline for temporal representation and Fourier for spatial representation, as it achieves the highest performance.

Limitations While our method demonstrates performance improvements, there still remain certain limitations.



Figure 5. Qualitative comparison on a large motion case with a spatial scale of $\times 1$ and a temporal scale of $\times 8$. Three interpolation results at $t = 0.25, 0.5, 0.625$ are shown.

As shown in Figure 5, existing C-STVSR models, including ours, still struggle with handling large motion. Moreover, the training process of C-STVSR models is time-consuming and computationally expensive. Addressing these challenges remains an open problem for future research.

5. Conclusions

In this paper, we proposed BF-STVSR, a novel framework for Continuous Spatial-Temporal Video Super Resolution (C-STVSR). We introduced two specialized position encoding modules: B-spline Mapper, which leverages B-spline basis functions for smooth and accurate temporal interpolation, and Fourier Mapper, which captures dominant spatial frequencies to effectively model fine-grained spatial details. Our analysis highlights that naive position encoding can degrade performance, particularly when paired with optical flow networks, emphasizing the importance of tailored encodings for spatial and temporal axes. Through extensive experiments, we show that BF-STVSR achieves state-of-the-art performance in PSNR and SSIM metrics across diverse datasets, demonstrating enhanced spatial detail, natural temporal consistency, and robustness under challenging conditions, including extreme out-of-distribution scales.

References

- [1] Wenbo Bao, Wei-Sheng Lai, Chao Ma, Xiaoyun Zhang, Zhiyong Gao, and Ming-Hsuan Yang. Depth-aware video frame interpolation. In *IEEE Conference on Computer Vision and Pattern Recognition*, 2019. 1, 5, 6
- [2] Jose Caballero, Christian Ledig, Andrew Aitken, Alejandro Acosta, Johannes Totz, Zehan Wang, and Wenzhe Shi. Real-time video super-resolution with spatio-temporal networks and motion compensation. In *Proceedings of the IEEE conference on computer vision and pattern recognition*, pages 4778–4787, 2017. 2
- [3] Kelvin C.K. Chan, Xintao Wang, Ke Yu, Chao Dong, and Chen Change Loy. Basicvsr: The search for essential components in video super-resolution and beyond. In *Proceedings of the IEEE conference on computer vision and pattern recognition*, 2021. 1, 5, 6
- [4] Kelvin C.K. Chan, Shangchen Zhou, Xiangyu Xu, and Chen Change Loy. BasicVSR++: Improving video super-resolution with enhanced propagation and alignment. In *IEEE Conference on Computer Vision and Pattern Recognition*, 2022. 1, 2
- [5] Yinbo Chen, Sifei Liu, and Xiaolong Wang. Learning continuous image representation with local implicit image function. In *CVPR*, pages 8628–8638, 2021. 1, 2, 5, 6
- [6] Yi-Hsin Chen, Si-Cun Chen, Yen-Yu Lin, and Wen-Hsiao Peng. Motif: Learning motion trajectories with local implicit neural functions for continuous space-time video super-resolution. In *Proceedings of the IEEE/CVF International Conference on Computer Vision*, pages 23131–23141, 2023. 2, 3, 4, 5, 6, 8
- [7] Zeyuan Chen, Yinbo Chen, Jingwen Liu, Xingqian Xu, Vidit Goel, Zhangyang Wang, Humphrey Shi, and Xiaolong Wang. Videoir: Learning video implicit neural representation for continuous space-time super-resolution. *Proceedings of the IEEE/CVF Conference on Computer Vision and Pattern Recognition*, 2022. 2, 3, 4, 5, 6
- [8] Xianhang Cheng and Zhenzhong Chen. Video frame interpolation via deformable separable convolution. In *Proceedings of the AAAI Conference on Artificial Intelligence*, pages 10607–10614, 2020. 1, 2, 3
- [9] Xianhang Cheng and Zhenzhong Chen. Multiple video frame interpolation via enhanced deformable separable convolution. *IEEE Transactions on Pattern Analysis and Machine Intelligence*, 44(10):7029–7045, 2021.
- [10] Myungsub Choi, Heewon Kim, Bohyung Han, Ning Xu, and Kyoung Mu Lee. Channel attention is all you need for video frame interpolation. In *Proceedings of the AAAI Conference on Artificial Intelligence*, pages 10663–10671, 2020. 1
- [11] Duolikun Danier, Fan Zhang, and David Bull. St-mfnet: A spatio-temporal multi-flow network for frame interpolation. In *Proceedings of the IEEE/CVF Conference on Computer Vision and Pattern Recognition*, pages 3521–3531, 2022. 2, 3
- [12] Zelin Gao, Weichen Dai, and Yu Zhang. Adaptive positional encoding for bundle-adjusting neural radiance fields. In *Proceedings of the IEEE/CVF International Conference on Computer Vision*, pages 3284–3294, 2023. 2
- [13] Shurui Gui, Chaoyue Wang, Qihua Chen, and Dacheng Tao. Featureflow: Robust video interpolation via structure-to-texture generation. In *Proceedings of the IEEE/CVF Conference on Computer Vision and Pattern Recognition*, pages 14004–14013, 2020. 1, 2
- [14] Muhammad Haris, Greg Shakhnarovich, and Norimichi Ukita. Space-time-aware multi-resolution video enhancement. In *Proceedings of the IEEE/CVF conference on computer vision and pattern recognition*, pages 2859–2868, 2020. 2
- [15] Xuecai Hu, Haoyuan Mu, Xiangyu Zhang, Zilei Wang, Tieniu Tan, and Jian Sun. Meta-sr: A magnification-arbitrary network for super-resolution. In *IEEE Conference on Computer Vision and Pattern Recognition (CVPR)*, 2019. 1
- [16] Kyong Hwan Jin Jaewon Lee, Kwang Pyo Choi. Learning local implicit fourier representation for image warping. *ECCV*, 2022. 2
- [17] Huaizu Jiang, Deqing Sun, Varun Jampani, Ming-Hsuan Yang, Erik Learned-Miller, and Jan Kautz. Super slo-mo: High quality estimation of multiple intermediate frames for video interpolation. In *IEEE/CVF Conference on Computer Vision and Pattern Recognition (CVPR)*, 2018. 5, 6
- [18] Tarun Kalluri, Deepak Pathak, Manmohan Chandraker, and Du Tran. Flavr: Flow-agnostic video representations for fast frame interpolation. In *Proceedings of the IEEE/CVF winter conference on applications of computer vision*, pages 2071–2082, 2023. 1, 2, 3
- [19] Subin Kim, Sihyun Yu, Jaeho Lee, and Jinwoo Shin. Scalable neural video representations with learnable positional features. *Advances in Neural Information Processing Systems*, 35:12718–12731, 2022. 2
- [20] Lingtong Kong, Boyuan Jiang, Donghao Luo, Wenqing Chu, Xiaoming Huang, Ying Tai, Chengjie Wang, and Jie Yang. Ifrnet: Intermediate feature refine network for efficient frame interpolation. In *Proceedings of the IEEE/CVF Conference on Computer Vision and Pattern Recognition*, pages 1969–1978, 2022. 2, 3
- [21] Hyeongmin Lee, Taeh Kim, Tae-young Chung, Daehyun Pak, Yuseok Ban, and Sangyoung Lee. Adacof: Adaptive collaboration of flows for video frame interpolation. In *Proceedings of the IEEE/CVF conference on computer vision and pattern recognition*, pages 5316–5325, 2020. 2
- [22] Jaewon Lee and Kyong Hwan Jin. Local texture estimator for implicit representation function. In *CVPR*, pages 1929–1938, 2022. 1, 2, 4
- [23] Jingyun Liang, Jiezhong Cao, Guolei Sun, Kai Zhang, Luc Van Gool, and Radu Timofte. Swinir: Image restoration using swin transformer. In *Proceedings of the IEEE/CVF international conference on computer vision*, pages 1833–1844, 2021. 2
- [24] Bee Lim, Sanghyun Son, Heewon Kim, Seungjun Nah, and Kyoung Mu Lee. Enhanced deep residual networks for single image super-resolution. In *Proceedings of the IEEE conference on computer vision and pattern recognition workshops*, pages 136–144, 2017. 2
- [25] Ce Liu and Deqing Sun. A bayesian approach to adaptive video super resolution. In *CVPR 2011*, pages 209–216, 2011. 5

- [26] Ying-Tian Liu, Yuan-Chen Guo, and Song-Hai Zhang. Enhancing multi-scale implicit learning in image super-resolution with integrated positional encoding. *arXiv preprint arXiv:2112.05756*, 2021. 2
- [27] Ben Mildenhall, Pratul P. Srinivasan, Matthew Tancik, Jonathan T. Barron, Ravi Ramamoorthi, and Ren Ng. Nerf: Representing scenes as neural radiance fields for view synthesis. In *ECCV*, 2020. 2, 4
- [28] Thomas Müller, Alex Evans, Christoph Schied, and Alexander Keller. Instant neural graphics primitives with a multi-scale convolutional neural network for dynamic scene deblurring. *ACM transactions on graphics (TOG)*, 41(4):1–15, 2022. 2
- [29] Seungjun Nah, Tae Hyun Kim, and Kyoung Mu Lee. Deep multi-scale convolutional neural network for dynamic scene deblurring. In *The IEEE Conference on Computer Vision and Pattern Recognition (CVPR)*, 2017. 5
- [30] Simon Niklaus and Feng Liu. Context-aware synthesis for video frame interpolation. In *Proceedings of the IEEE conference on computer vision and pattern recognition*, pages 1701–1710, 2018. 2
- [31] Simon Niklaus and Feng Liu. Softmax splatting for video frame interpolation. In *Proceedings of the IEEE/CVF conference on computer vision and pattern recognition*, pages 5437–5446, 2020. 2, 3, 4
- [32] Byeonghyun Pak and Kyong Hwan Jin. B-spline texture coefficients estimator for screen content image super-resolution. In *CVPR*, 2023. 1, 2, 4
- [33] Junheum Park, Chul Lee, and Chang-Su Kim. Asymmetric bilateral motion estimation for video frame interpolation. In *Proceedings of the IEEE/CVF international conference on computer vision*, pages 14539–14548, 2021. 2, 3
- [34] Nasim Rahaman, Aristide Baratin, Devansh Arpit, Felix Draxler, Min Lin, Fred Hamprecht, Yoshua Bengio, and Aaron Courville. On the spectral bias of neural networks. In *International conference on machine learning*, pages 5301–5310. PMLR, 2019. 2, 4
- [35] Fitsum Reda, Janne Kontkanen, Eric Tabellion, Deqing Sun, Caroline Pantofaru, and Brian Curless. Film: Frame interpolation for large motion. In *European Conference on Computer Vision (ECCV)*, 2022. 2, 3
- [36] Mehdi SM Sajjadi, Raviteja Vemulapalli, and Matthew Brown. Frame-recurrent video super-resolution. In *Proceedings of the IEEE conference on computer vision and pattern recognition*, pages 6626–6634, 2018. 2
- [37] Wenzhe Shi, Jose Caballero, Ferenc Huszár, Johannes Totz, Andrew P Aitken, Rob Bishop, Daniel Rueckert, and Zehan Wang. Real-time single image and video super-resolution using an efficient sub-pixel convolutional neural network. In *Proceedings of the IEEE conference on computer vision and pattern recognition*, pages 1874–1883, 2016. 2
- [38] Zhihao Shi, Xiangyu Xu, Xiaohong Liu, Jun Chen, and Ming-Hsuan Yang. Video frame interpolation transformer. In *Proceedings of the IEEE/CVF Conference on Computer Vision and Pattern Recognition*, pages 17482–17491, 2022. 1, 2
- [39] Shuochen Su, Mauricio Delbracio, Jue Wang, Guillermo Sapiro, Wolfgang Heidrich, and Oliver Wang. Deep video deblurring for hand-held cameras. In *2017 IEEE Conference on Computer Vision and Pattern Recognition (CVPR)*, pages 237–246, 2017. 5
- [40] Shuochen Su, Mauricio Delbracio, Jue Wang, Guillermo Sapiro, Wolfgang Heidrich, and Oliver Wang. Deep video deblurring for hand-held cameras. In *Proceedings of the IEEE Conference on Computer Vision and Pattern Recognition*, pages 1279–1288, 2017. 5
- [41] Matthew Tancik, Pratul Srinivasan, Ben Mildenhall, Sara Fridovich-Keil, Nithin Raghavan, Utkarsh Singhal, Ravi Ramamoorthi, Jonathan Barron, and Ren Ng. Fourier features let networks learn high frequency functions in low dimensional domains. *Advances in neural information processing systems*, 33:7537–7547, 2020. 2, 4
- [42] Zachary Teed and Jia Deng. Raft: Recurrent all-pairs field transforms for optical flow. In *Computer Vision—ECCV 2020: 16th European Conference, Glasgow, UK, August 23–28, 2020, Proceedings, Part II 16*, pages 402–419. Springer, 2020. 2, 4, 7, 8
- [43] Yapeng Tian, Yulun Zhang, Yun Fu, and Chenliang Xu. Tdan: Temporally-deformable alignment network for video super-resolution. In *Proceedings of the IEEE/CVF conference on computer vision and pattern recognition*, pages 3360–3369, 2020. 1
- [44] Hua Wang, Dewei Su, Chuangchuan Liu, Longcun Jin, Xianfang Sun, and Xinyi Peng. Deformable non-local network for video super-resolution. *IEEE Access*, 7:177734–177744, 2019. 1
- [45] Peng-Shuai Wang, Yang Liu, Yu-Qi Yang, and Xin Tong. Spline positional encoding for learning 3d implicit signed distance fields. In *Proceedings of the Thirtieth International Joint Conference on Artificial Intelligence, IJCAI-21*, pages 1091–1097. International Joint Conferences on Artificial Intelligence Organization, 2021. Main Track. 2
- [46] Xintao Wang, Kelvin C.K. Chan, Ke Yu, Chao Dong, and Chen Change Loy. Edvr: Video restoration with enhanced deformable convolutional networks. In *The IEEE Conference on Computer Vision and Pattern Recognition Workshops (CVPRW)*, 2019. 1, 5, 6
- [47] Xiaoyu Xiang, Yapeng Tian, Yulun Zhang, Yun Fu, Jan P. Allebach, and Chenliang Xu. Zooming slow-mo: Fast and accurate one-stage space-time video super-resolution. In *IEEE/CVF Conference on Computer Vision and Pattern Recognition (CVPR)*, pages 3370–3379, 2020. 1, 2, 5, 6
- [48] Jun Xiao, Zihang Lyu, Cong Zhang, Yakun Ju, Changjian Shui, and Kin-Man Lam. Towards progressive multi-frequency representation for image warping. In *Proceedings of the IEEE/CVF Conference on Computer Vision and Pattern Recognition*, pages 2995–3004, 2024. 2
- [49] Gang Xu, Jun Xu, Zhen Li, Liang Wang, Xing Sun, and Mingming Cheng. Temporal modulation network for controllable space-time video super-resolution. In *IEEE/CVF Conference on Computer Vision and Pattern Recognition (CVPR)*, 2021. 5, 6
- [50] Xiangyu Xu, Li Siyao, Wenxiu Sun, Qian Yin, and Ming-Hsuan Yang. Quadratic video interpolation. In *NeurIPS*, 2019. 1, 5, 6

- [51] Xingqian Xu, Zhangyang Wang, and Humphrey Shi. Ultrasr: Spatial encoding is a missing key for implicit image function-based arbitrary-scale super-resolution. *arXiv preprint arXiv:2103.12716*, 2021. [2](#)
- [52] Tianfan Xue, Baian Chen, Jiajun Wu, Donglai Wei, and William T Freeman. Video enhancement with task-oriented flow. *International Journal of Computer Vision (IJCV)*, 127(8):1106–1125, 2019. [7](#)
- [53] Guozhen Zhang, Yuhan Zhu, Haonan Wang, Youxin Chen, Gangshan Wu, and Limin Wang. Extracting motion and appearance via inter-frame attention for efficient video frame interpolation. In *Proceedings of the IEEE/CVF Conference on Computer Vision and Pattern Recognition*, pages 5682–5692, 2023. [2](#), [3](#)
- [54] Yulun Zhang, Kungpeng Li, Kai Li, Lichen Wang, Bineng Zhong, and Yun Fu. Image super-resolution using very deep residual channel attention networks. In *Proceedings of the European conference on computer vision (ECCV)*, pages 286–301, 2018. [2](#)